



UNIVERSITY OF LEEDS

This is a repository copy of *Modelling ruptures of buried high pressure dense phase CO<sub>2</sub> pipelines in carbon capture and storage applications - Part I. Validation.*

White Rose Research Online URL for this paper:  
<http://eprints.whiterose.ac.uk/82921/>

Version: Accepted Version

---

**Article:**

Wareing, CJ, Fairweather, M, Falle, SAEG et al. (1 more author) (2015) Modelling ruptures of buried high pressure dense phase CO<sub>2</sub> pipelines in carbon capture and storage applications - Part I. Validation. *International Journal of Greenhouse Gas Control*, 42. 701 - 711. ISSN 1750-5836

<https://doi.org/10.1016/j.ijggc.2015.01.020>

---

© 2015, Elsevier. Licensed under the Creative Commons Attribution-NonCommercial-NoDerivatives 4.0 International  
<http://creativecommons.org/licenses/by-nc-nd/4.0/>

**Reuse**

Unless indicated otherwise, fulltext items are protected by copyright with all rights reserved. The copyright exception in section 29 of the Copyright, Designs and Patents Act 1988 allows the making of a single copy solely for the purpose of non-commercial research or private study within the limits of fair dealing. The publisher or other rights-holder may allow further reproduction and re-use of this version - refer to the White Rose Research Online record for this item. Where records identify the publisher as the copyright holder, users can verify any specific terms of use on the publisher's website.

**Takedown**

If you consider content in White Rose Research Online to be in breach of UK law, please notify us by emailing [eprints@whiterose.ac.uk](mailto:eprints@whiterose.ac.uk) including the URL of the record and the reason for the withdrawal request.



[eprints@whiterose.ac.uk](mailto:eprints@whiterose.ac.uk)  
<https://eprints.whiterose.ac.uk/>

# Modelling ruptures of buried high pressure dense phase CO<sub>2</sub> pipelines in carbon capture and storage applications - Part I. validation

Christopher J. Wareing<sup>a,b,\*</sup>, Michael Fairweather<sup>a</sup>, Samuel A.E.G. Falle<sup>c</sup>,  
Robert M. Woolley<sup>a</sup>

<sup>a</sup>*School of Chemical and Process Engineering, University of Leeds, Leeds LS2 9JT, UK.*

<sup>b</sup>*School of Physics and Astronomy, University of Leeds, Leeds LS2 9JT, UK.*

<sup>c</sup>*School of Mathematics, University of Leeds, Leeds LS2 9JT, UK.*

---

## Abstract

Carbon dioxide (CO<sub>2</sub>) capture and storage presents a short-term option for significantly reducing the amount of CO<sub>2</sub> released into the atmosphere and mitigating the effects of climate change. To this end, National Grid initiated the COOLTRANS research programme to consider the pipeline transportation of high pressure dense phase CO<sub>2</sub>, including the development and application of a mathematical model for predicting the sonic near-field dispersion of pure CO<sub>2</sub> following the venting or failure of such a pipeline. Here, the application of this model to the rupture of a buried pipeline is considered and compared to experimental data obtained through the COOLTRANS programme. The rupture experiment was performed on a 230m length of 152mm external diameter pipeline with 300 mm soil cover, equivalent to approximately 1/4 scale when compared to the proposed full-scale 600 mm

---

\*Corresponding author. Tel: +44 113 343 3871. Fax: +44 113 343 5090

*Email address:* C.J.Wareing@leeds.ac.uk (Christopher J. Wareing)

*URL:* <http://www.maths.leeds.ac.uk/~cjw> (Christopher J. Wareing)

(24-inch) diameter pipelines with 1.2 m soil cover on average proposed in the UK. The experiment was performed in a pre-formed crater based on experimentally formed craters in other experiments. The comparison demonstrates reasonable quantitative and qualitative agreement. Such validated dispersion flow, to be applied to full-scale rupture modelling in Part II, defines novel, robust, thermodynamically accurate multi-phase source conditions, that enable far-field computational fluid dynamics studies and feed into pragmatic quantified risk assessment models.

---

## 1. Introduction

Carbon dioxide (CO<sub>2</sub>) capture and storage (CCS) refers to a set of technologies designed to reduce CO<sub>2</sub> emissions from large industrial point sources of emission, such as coal-fired power stations, in order to mitigate greenhouse gas production. The technology involves capturing CO<sub>2</sub> and then storing it in a reservoir, instead of allowing its release to the atmosphere, where it contributes to climate change. Once captured, the CO<sub>2</sub> is transported and stored, typically underground, or used for processes such as enhanced oil recovery.

National Grid initiated the TRANSportation of Liquid CO<sub>2</sub> research programme (COOLTRANS) (Cooper, 2012) in order to address knowledge gaps relating to the safe design and operation of onshore pipelines for transporting dense phase CO<sub>2</sub> from industrial emitters in the UK to storage sites offshore. This includes developing the capability for modelling the low-probability, high-impact worst case scenario - an accidental release from a buried pipeline that contains CO<sub>2</sub> in the dense phase. Learning from these studies can sub-

sequently be combined with a range of other information to inform front-end engineering design (FEED) activities and to develop an appropriate quantified risk assessment (QRA) for a dense phase CO<sub>2</sub> pipeline, currently underway in the UK for two CCS projects (Peterhead, and Don Valley, into which this work specifically contributed). With regard to modelling the worst case scenario, the programme includes theoretical studies by University College London (UCL), the University of Leeds and University of Warwick, carried out in parallel to provide “state of the art” numerical models that connect together in full chain dispersion modelling for the outflow (UCL), near-field dispersion behaviour (Leeds) and far-field dispersion behaviour (Warwick) associated with below ground CO<sub>2</sub> pipelines that are ruptured or punctured. Experimental work and studies using currently available practical models for risk assessment are being carried out by DNV GL (Allason et al., 2012; Cosham et al., 2012). The experimental work has provided data against which the modellers can compare their predictions.

In this paper, the Leeds mathematical model (Wareing et al., 2013a), previously validated for free releases into air (Woolley et al., 2013; Wareing et al., 2014a), small-scale laboratory releases and dry ice particle behaviour (Wareing et al., 2013b) and punctures of buried pipelines (Wareing et al., 2014b), is validated against COOLTRANS experimental data from a rupture of a buried pipeline with external diameter of 152mm and wall thickness of 11mm, resulting in an internal diameter of approximately 130mm. This is approximately 1/4-scale when compared to the 600mm diameter pipelines proposed in the Don Valley CCS project referred to above and henceforth in this article the experiment will be referred to as 1/4-scale. Ruptures occur in

pipelines for a number of reasons - from human interference to pipeline defects (Cosham et al., 2012b). The validation described in this paper represents a considerable step toward the goal of developing a modelling capability for the transient rupture of a buried pipeline.

In the next section we review the background literature. In the following Section 3, we present the experimental details of this 1/4 scale rupture experiment. In Section 4, we summarise the model and numerical method. Numerical predictions of this 1/4-scale rupture are presented in Section 5 and compared with experimental data. The comparisons are further discussed in Section 6 and the limits of applicability are discussed in Section 7, Finally, brief conclusions are presented in Section 8. Part II. of this two-paper series will apply the model to a full-scale rupture and present numerical simulations of a full-scale transient decompression, as well as sensitivity studies with regard to expected variations of the shape of the crater. As experimental data of the type used here for validation is not currently available for full-scale ruptures, such a sensitivity study is very valuable.

## **2. Background**

In this section, we consider the growing number of recent publications that have examined the release and dispersion of CO<sub>2</sub>, revisiting our review from Wareing et al. (2014a) that summarised the depth provided by Dixon et al. (2012) in the light of new and related additions to the literature.

A study by MMI Engineering (Dixon and Hasson, 2007) presented dispersion simulations employing the ANSYS-CFX computational fluid dynamics (CFD) code. Solid CO<sub>2</sub> particles were simulated by a scalar representing

the particle concentration, in order to avoid additional computing associated with Lagrangian particle tracking. Dixon et al. (2012) note that this method assumed a constant particle diameter and temperature (at the sublimation temperature of  $-78.9^{\circ}\text{C}$  in order to calculate heat and mass exchange between the particles and the gas phase. In a following publication (Dixon et al., 2009), particles were modelled via a Lagrangian particle tracking method, but were still assumed to be at the sublimation temperature. Dixon et al. (2012) note that since the rate of sublimation increases as particle size decreases, an improved distribution of the source of the  $\text{CO}_2$  gas resulting from particle sublimation could be obtained by allowing for varying particle size and for the fact that temperature is expected to fall below the sublimation temperature in the near-field of a release.

In 2011, Webber (2011) presented a methodology for extending existing two-phase homogeneous integral models for flashing jets to the three-phase case for  $\text{CO}_2$ . Webber noted that as the flow expands from the reservoir conditions to atmospheric pressure, temperature, density and the jet cross-sectional area would vary continuously through the triple point, whilst the mass and momentum would be conserved. This led to the conclusion that there must be a discontinuity in the enthalpy and  $\text{CO}_2$  condensed phase fraction, in a similar manner to the energy change associated with passing through a hydraulic jump. In the development of our composite equation of state for modelling  $\text{CO}_2$  near-field sonic dispersion (Wareing et al., 2013a), we confirmed this in a conservative shock capturing CFD code and highlighted the importance of fully accounting for the solid phase and latent heat of fusion; the near-field structure of the jet as well as the fraction of solid phase

material is different when this is correctly accounted for.

Two recent papers (Witlox et al., 2009, 2011) have discussed the application of the software package PHAST to CO<sub>2</sub> release and dispersion modelling. In the first of these, Witlox et al. (2009) described an extension to the existing model in PHAST (v. 6.53.1) to account for the effects of solid CO<sub>2</sub>, including the latent heat of fusion. The modifications to the model consisted principally of changing the way in which equilibrium conditions were calculated in the expansion of CO<sub>2</sub> to atmospheric pressure. This was done in order to ensure that below the triple point, conditions followed the sublimation curve in the phase diagram, rather than extrapolating the evaporation curve (which diverges considerably from reality, hence the limitations of the Peng and Robinson (1976) and Span and Wagner (1996) equations of state to above the triple point only). In the second paper (Witlox et al., 2011), the results of sensitivity tests were reported for both liquid and supercritical CO<sub>2</sub> releases from vessels and pipes calculated with the revised PHAST model. The public release of the CO2PIPETRANS datasets and associated industrial projects, e.g. (Ahmad et al., 2013), has validated the development of this approach, which we also adopted in part for our composite equation of state (Wareing et al., 2013a).

E.ON have published a number of studies in support of their proposed CCS programme (Mazzoldi et al., 2008a,b, 2011; Hill et al., 2011). Of these, the most relevant to this work are Mazzoldi et al. (2011) and Hill et al. (2011). These consider atmospheric dispersion from pipeline and vessel releases. The former paper compared simulations from the heavy gas model ALOHA to the CFD model Fluidyn-Panache. Only the gaseous stage of the release was

modelled. In the second work (Hill et al., 2011), the authors presented CFD and PHAST simulations of dense-phase CO<sub>2</sub> releases from a 0.5m diameter hole in a pipeline, located at an elevation of 5m above level ground. Steady-state flow rates were calculated at the orifice assuming saturated conditions. CFD simulations were performed using the ANSYS-CFX code with a Lagrangian particle tracking model for the solid CO<sub>2</sub> particles, with three size distributions: 10 to 50 micrometers, 50 to 100 micrometers and 50 to 150 micrometers. Simulations were also performed without particles. Their results showed that sublimation of the particles led to a cooling of the CO<sub>2</sub> plume, affecting dispersion behaviour, although the results were relatively insensitive to particle size. Gas concentrations downwind from the release were reportedly somewhat lower using PHAST (v 6.6) as compared to the CFD results. No comparison to experiment was performed.

Dixon et al. (2012) point out that it appears that in the Lagrangian model of Hill et al. (2011) their particle tracks followed closely the plume centre-line, rather than being spread throughout the plume. Dixon et al. (2012) noted that turbulence will have the effect of bringing particles into contact with parts of the jet at a higher temperature and lower CO<sub>2</sub> concentration, thereby tending to increase the rate of sublimation and increase the radius of the region cooled by the subliming particles. In their work, Dixon et al. (2012) included turbulent dispersion effects in the CFX model. Further, they assumed that the solid particles are much smaller with an initial particle diameter of 5 micrometers. They made that choice based on an analysis of CO<sub>2</sub> experiments. In addition, this particle size distribution is supported by the model recently developed by Hulsbosch-Dam et al. (2012b,a), which

suggested that the particle diameter would be around 5 micrometers for CO<sub>2</sub> releases at a pressure of 100bar, when the difference between the CO<sub>2</sub> and ambient temperatures is around 80°C. They stated that the effect of having smaller particles in their model was likely to cause more rapid sublimation, which should produce a more significant reduction in gas temperature in the jet. Recent examination of particle size distribution in releases of supercritical CO<sub>2</sub> from high pressure has shown that even smaller particles immediately post Mach shock are indeed the case (Liu et al., 2012b), on the order of a few micrometers, which we have also been able to confirm in laboratory releases from the liquid phase (Wareing et al., 2013b).

Dixon et al. (2012) employ a Bernoulli method in their recent paper which they found "to provide reasonable predictions of the flow rate for the sub-cooled liquid CO<sub>2</sub> releases". Differences were apparent between the integral model and the CFD model results. The integral model predicted temperatures that they noted were too low in the near-field, and which then returned too rapidly to atmospheric levels (see Dixon et al. (2012) Figure 3.). The CFD model was noted to be in general better, although in the very near-field (< 10m from the orifice) it was still not clear whether this was the case. Further, the CFD model appears to under-predict the spreading rate of the jet.

Liu et al. (2014) present simulations of free-jet CO<sub>2</sub> dispersion from high pressure pipelines using a real gas equation of state - specifically the Peng-Robinson (Peng and Robinson, 1976) equation. They obtain good agreement compared to the limited data available from the CO<sub>2</sub>PIPETRANS datasets (no data is available close to the sonic expansion region), but do not model

the solid phase of CO<sub>2</sub> and hence are limited to predicting supercritical releases that do not cool below the triple point. Developments are noted to be underway to consider the solid phase.

Wareing et al. (2013a) present a composite equation of state for the modelling of high pressure liquid CO<sub>2</sub> releases that does account for phase changes and the solid phase and then go on to validate against venting releases from the CO2PIPEHAZ project (Woolley et al., 2013) and the COOLTRANS research programme (Wareing et al., 2014a). The model demonstrates good quantitative and qualitative agreement with the experimental data regarding temperature and concentration in the near- and far-field. Recently, Wareing et al. (2014b) have applied the same model to punctures of buried high pressure dense phase pipelines and again compare the numerical simulations to experimental data. The model shows reasonable agreement with the data, predicting jet temperatures, structures and behaviour, as well as predicting particle behaviour. Very recently, Woolley et al. (2014) published a paper linking the elements of the EU FP7 project CO2PIPEHAZ ([www.co2pipehaz.eu](http://www.co2pipehaz.eu)) together, for the first time numerically modelling a complete chain rupture and consequent dispersion event in realistic topography, including pipeline decompression linked to near-field sonic shock-capturing simulation of the flow from the pipe ends through the crater linked into the far-field, where constant source conditions on a plane above the crater were taken as input into FLACS and ANSYS-CFX simulations. These source conditions were taken as constant source conditions and the transient nature of the near-field decompression was not modelled. Gant et al. (2014) had previously considered the validation of FLACS and ANSYS-CFX in the far-

field for this application, using Leeds predictions for the near-field, albeit again modified for input into such commercial software. Wen et al. (2013) presented a number of far-field simulations of venting and horizontal above ground releases, with successful validation, also using the Leeds model for input conditions, but with less modification for input into their software. In this paper, we now address the necessary validation of the Leeds near-field mathematical model for application to rupture releases, so that it can be reliably used for input into far-field simulations for full-scale pipeline ruptures.

### **3. Experimental details**

As part of the COOLTRANS research programme, a number of experimental studies were carried out (Allason et al., 2012; Cosham et al., 2012). Two types of experiment were defined: Category 1 cases for the demonstration of methodology and Category 2 cases for model development and validation. Here, the fourth in the Category 1 series is considered solely for the purpose of validating the numerical approach to modelling near-field regions of full-scale pipeline ruptures. It involves a transient release from the opposed ends of sections of below ground pipe that are initially connected to separate reservoirs filled with CO<sub>2</sub> in the dense phase, designed to study how a rupture in a below ground pipeline would behave. The experiments were performed at the DNV GL Spadeadam facility in Cumbria, U.K. We summarise the details relevant to the numerical modelling and validation aim of this paper in the rest of this section, including the experimental rig, installation and test procedure. Complete details of the experimental programme are beyond the scope of this paper.

### *3.1. Experimental rig*

A 230 m long length of 152 mm (6 inch) external diameter pipeline, nominally ‘1/4 scale’ compared to anticipated full-scale 600 mm diameter pipelines, with 11 mm wall thickness was buried horizontally at a depth of 300 mm from the surface to the top of the pipe. This depth was selected as it is 1/4 the average 1.2 m depth of pipelines proposed in the Don Valley CCS Project. Each end was connected through remotely-operated valves to separate 914 mm (36 inch) external diameter ‘reservoir’ pipes. A 3 m long test section was removed from the middle of the 230m pipeline. The open ends created by the removal of this test section were held in place by buried concrete anchor blocks.

The particular release considered here took place into a preformed crater below ground, based on previous experiments. There was no soil backfill in the crater and so the release took place unhindered into air. The dimensions of the crater are shown in Figure 1 and constitute a 1/4 scaling of a full-scale rupture event in a 600 mm (24 inch) diameter pipeline, based on information provided from DNV GL.

### *3.2. Instrumentation*

The 152 mm internal diameter pipeline was instrumented with pressure transducers and thermocouples. Measurements were made above the crater of the temperature within the dispersing CO<sub>2</sub> cloud that was produced. Specifically, an array of thermocouples was placed in a 1 m spaced grid layout on a horizontal plane 1 m above the crater, centred on the crater. The lay-out of the temperature sensors on this array is shown in Figure 2. It is to these experimental data that comparisons are made in later sections of this paper.

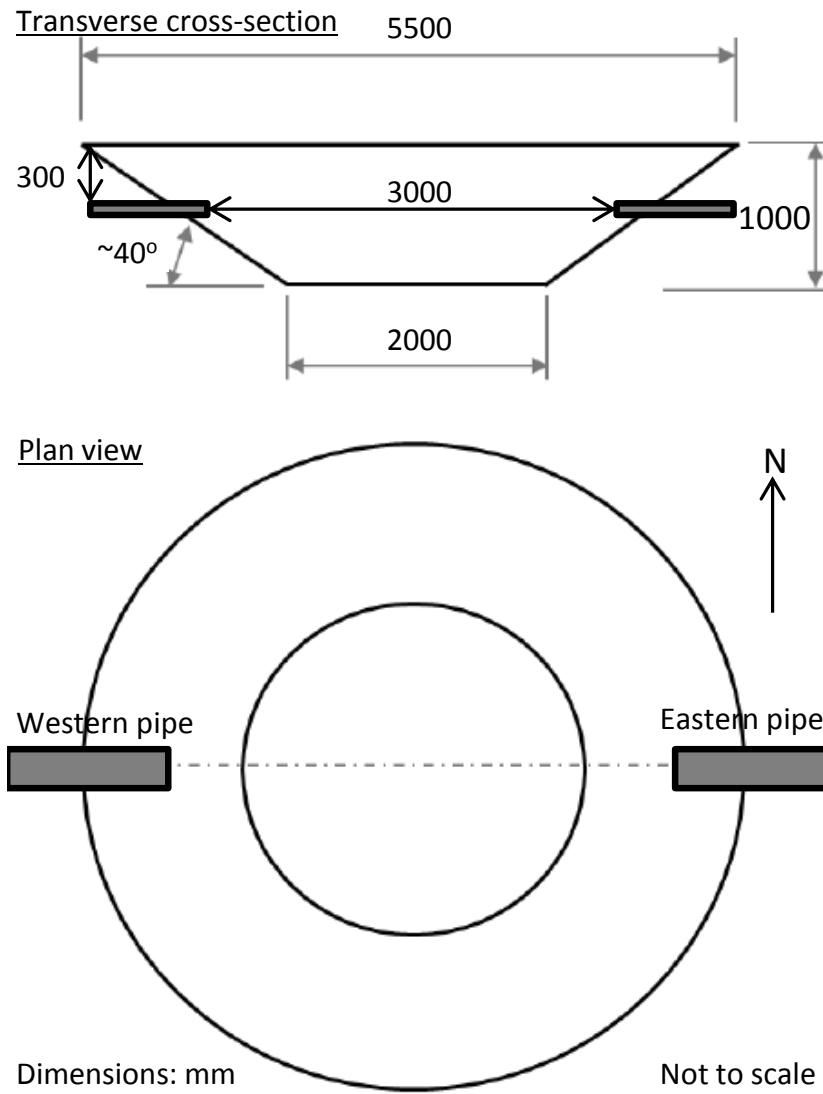


Figure 1: Dimensions of the crater used to examine a full-scale rupture of a high pressure dense phase CO<sub>2</sub> pipeline.

Measurements of concentration were also made at ground level in arcs away from the crater, but these far-field measurements are too far from the crater to be modelled in the near-field simulation and beyond the aim of near-field

validation of the mathematical model in this paper.

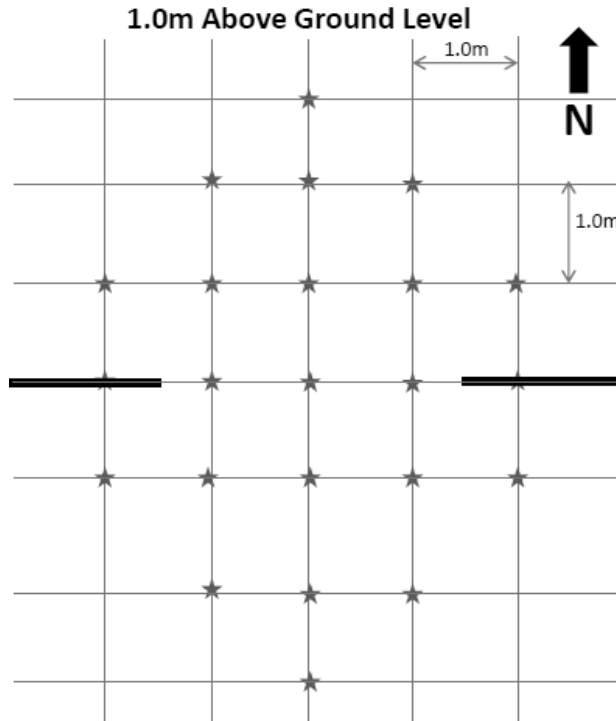


Figure 2: A schematic of the array of temperature sensors 1m above the crater.

### 3.3. Test procedure

Once the desired pressure and temperature had been achieved in the reservoirs (see later descriptions and Table 1) and the preparations completed, the remotely-operated valves were triggered to allow flow out of the two opposed, full-bore, open pipe ends.  $\text{CO}_2$  flowed into the crater and emerged from it to disperse in the atmosphere. The release was observed to undergo a rapid decay initially, as the  $\text{CO}_2$  in the 230 m pipeline depressurised to saturated conditions, followed by a very slowly decaying period as the 'reservoirs' de-

pressurised. After 450 seconds the experiment was terminated by closing the remotely-operated valves.

Consistent measurements of temperature at a rate of 10 measurements per second were obtained on the plane above the crater and it is to these data that the numerical predictions are compared in later sections. The experimental data has a variance on each measurement during the relevant time period of 30 s to 60 s of a few degrees. The temperature sensors are accurate in the observed temperature range to within  $\pm 5^\circ\text{C}$  at worst, hence throughout all the plots given later the experimental measurements are plotted with 5 degree error bars. The plotted temperature is the simple average for that particular sensor during the 30 s to 60 s period. The response time of the sensors is certainly less than this averaging period. From the sensor traces, it is possible to estimate that the response time to reach 80% of the temperature change is up to 5 seconds. Going from cold to hot following the release is considerably longer, due to possible ice formation around the connections, but this is long beyond the averaging period.

#### **4. Numerical method**

The numerical approach is essentially the same as that adopted and validated in our earlier papers (Wareing et al., 2013a,b, 2014a,b; Woolley et al., 2013, 2014) and we refer the reader to these articles for detailed information and validation of our approach for free releases and punctures of buried pipelines. In the following subsections, we summarise our method.

#### 4.1. Reynolds-averaged Navier-Stokes model

The Reynolds-averaged Navier-Stokes (RANS) equations, closed with a compressibility-corrected  $k$ - $\epsilon$  turbulence model, employed in this work are:

$$\frac{\partial \rho}{\partial t} + \nabla \cdot (\rho \mathbf{u}) = 0 \quad (1)$$

$$\frac{\partial \rho C}{\partial t} + \nabla \cdot (\rho C \mathbf{u}) - \nabla \cdot (\mu_T \nabla C) = 0 \quad (2)$$

$$\frac{\partial \rho \mathbf{u}}{\partial t} + \nabla \cdot (\rho \mathbf{u} \mathbf{u}) + \nabla P - \nabla \cdot \boldsymbol{\tau} = \mathbf{s}_p \quad (3)$$

$$\frac{\partial E}{\partial t} + \nabla \cdot [(E + P) \mathbf{u} - \mathbf{u} \cdot \boldsymbol{\tau}] - \nabla \cdot (\mu_T T \nabla S) = 0 \quad (4)$$

$$\frac{\partial \rho k}{\partial t} + \nabla \cdot (\rho k \mathbf{u}) - \nabla \cdot (\mu_T \nabla k) = s_k \quad (5)$$

$$\frac{\partial \rho \epsilon}{\partial t} + \nabla \cdot (\rho \epsilon \mathbf{u}) - \nabla \cdot (\mu_\epsilon \nabla \epsilon) = s_\epsilon \quad (6)$$

where the variables have their usual meanings, noting that the vector velocity is expressed in bold as  $\mathbf{u}$  and  $S$  is the entropy per unit mass. The turbulent diffusion coefficients are

$$\mu_T = \rho C_\mu \frac{k^2}{\epsilon}, \quad \mu_\epsilon = \frac{\mu_T}{1.3}, \quad C_\mu = 0.09. \quad (7)$$

The turbulence production term is

$$P_t = \mu_T \left[ \frac{\partial u_i}{\partial x_j} \left( \frac{\partial u_i}{\partial x_j} + \frac{\partial u_j}{\partial x_i} \right) \right] - \frac{2}{3} \nabla \cdot \mathbf{u} (\rho k + \mu_T \nabla \cdot \mathbf{u}), \quad (8)$$

where the summation convention has been assumed. The momentum equation source term,  $\mathbf{s}_p$ , is zero in Cartesian coordinates. The  $k$  source term is

$$s_k = P_t - \rho \epsilon \quad (9)$$

whilst the  $\epsilon$  source term is

$$s_\epsilon = \frac{\epsilon}{k}(C_1 P_t - C_2 \rho \epsilon), \quad C_1 = 1.4, \quad C_2 = 1.94. \quad (10)$$

The turbulent stress tensor,  $\tau$ , is

$$\tau_{ij} = \mu_T \left( \frac{\partial u_i}{\partial x_j} + \frac{\partial u_j}{\partial x_i} \right) - \frac{2}{3} \delta_{ij} (\mu_T \nabla \cdot \mathbf{u} + \rho k). \quad (11)$$

The k- $\epsilon$  turbulence model described here is coupled to a compressibility dissipation rate correction proposed by Sarkar et al. (1991). Comparisons of model predictions with this correction and experimental data have shown significant improvements over results derived using the standard k- $\epsilon$  approach for moderately and highly under-expanded jets of the type under consideration here (Cumber et al., 1994, 1995).

#### 4.2. Equation of state

The composite equation of state recently described in Wareing et al. (2013a) is employed. This composite method predicts the thermophysical properties of the three phases of CO<sub>2</sub> for the range of temperatures of relevance to CO<sub>2</sub> dispersion from releases at sonic velocities, of interest to the CCS industry. This new equation of state has been developed in such a way that is convenient for computational fluid dynamic applications; the gas phase is computed from the Peng-Robinson equation of state (Peng and Robinson, 1976), and the liquid and condensed phases from tabulated data generated with the Span & Wagner equation of state (Span and Wagner, 1996) and the DIPPR<sup>®</sup> Project 801 database (<http://www.aiche.org/dippr/>), academic access to which can be gained through the Knovel library (<http://why.knovel.com>). Pressure, gas and condensed phase densities, sound speed and internal energy

have all been tabulated against temperature on the saturation line between  $-173.15^{\circ}\text{C}$  (100K) and the critical temperatures, providing the basis for a fully functional form for differentiation, interpolation and extrapolation in numerical simulations. No discontinuity or loss of accuracy at the critical point or anywhere along the saturation curve has been encountered by using this composite approach with different equations of state, as the authors have ensured that the Helmholtz free energy has continuous first derivatives.

#### *4.3. Implementation*

The composite equation of state is implemented within a homogeneous equilibrium model into MG, an adaptive mesh refinement (AMR) RANS hydrodynamic code developed by Falle (1991). The code employs an upwind, conservative shock-capturing scheme and is able to employ multiple processors through parallelisation with the message passing interface (MPI) library. Integration proceeds according to a second-order accurate Godunov method (Godunov, 1959). In this case, a Harten Lax van-Leer (van Leer, 1977; Harten et al., 1983) (HLL) Riemann solver was employed to aid the implementation of complex equations of state. The disadvantage of the HLL solver is that it is more diffusive for contact discontinuities; this is not important here since the contact discontinuities are in any case diffused by the artificial viscosity. The artificial viscosity is required to ensure shocks travel at the correct speed in all directions and is at a very low level, decreasing proportionally with increasing resolution.

#### *4.4. Adaptive meshing strategy*

The AMR method (Falle, 2005) employs an unstructured grid approach, requiring an order of magnitude less memory and giving an order of magnitude faster computation times than structured grid AMR. The two coarsest levels - 0 and 1 - cover the whole computational domain; finer grids need not do so. Refinement or derefinement depends on a given tolerance. Where there are steep gradients of variable magnitudes such as at flow boundaries or discontinuities such as the Mach disc, this automated meshing strategy allows the mesh to be more refined than in areas of the free stream in the surrounding fluid. Each layer is generated from its predecessor by doubling the number of computational cells in each spatial direction. This technique enables the generation of fine grids in regions of high spatial and temporal variation, and conversely, relatively coarse grids where the flow field is numerically smooth. Defragmentation of the AMR grid in hardware memory was performed at every time-step, gaining further speed improvements for negligible cost through reallocation of cells into consecutive memory locations. The simulations presented below employed 5 levels of AMR and hence a low level of artificial viscosity.

Steady state flows were achieved by running the simulations until the flow out of the top of the crater did not change and the integrated mass-flux out of the crater matched the integrated mass-flux into the crater from the combined pipe ends. The simulations presented hereafter are at this stage. The simulations are also convergent, having been tested with higher AMR resolutions, and show little variation with pressure, temperature and velocity variation at the inlets.

#### *4.5. Initial conditions*

In computationally simulating the test described above, we employed a three-dimensional Cartesian coordinate domain. The simulation was performed ‘blind’ by the modellers in the COOLTRANS research programme, i.e. they knew only the design specification of the experiment, not any details of the level of success or quality of data obtained in the actual experiment. For this case, in the interest of timely results in the COOLTRANS programme and because the conditions in the upstream reservoirs were almost certainly stratified, with a bottom offtake, hence making modelling difficult for a pure pipeline model, inlet conditions at the pipe ends were provided by DNV GL. Complete predictions of the entire pipeline decompression were not necessary for this modelling and were not provided. It was modelled as a discharge from a stratified vessel with the actual length of 150 mm pipe acting as an offtake at the bottom of the reservoir. Homogeneous equilibrium was assumed for the flow in the 150 mm pipe and its outlet, taking saturated liquid conditions in the vessel at the initial reservoir temperature. Choked flow was assumed at the pipe exit. The pressure losses along the pipe were accounted for, but the dynamic changes were not modelled properly, so the flow was treated as varying slowly - an assumption confirmed by the experimental observations. The model used was a proprietary version (Cumber, 2001) derived from an original DIERS model that has been extended to deal with CO<sub>2</sub> and allows for homogeneous flow in a pipe connected to the reservoir. Details of the decompression track on a phase diagram are similar to those shown for liquid conditions in figure 7 of Wareing et al. (2013a). See also figure 1 of that paper for a schematic of the phase diagram of CO<sub>2</sub>. Given

that the experiment was designed such that the inlet conditions would be the same at both pipe ends, only a quarter crater was simulated in order to save computational effort and reach a steady state prediction in reasonable computing time. An agreed snapshot was simulated at  $t = 42$  s into the release, as the near-field computational simulation of the entire 450 s experiment is numerically challenging. Even simulating the single snapshot required several days on 128 cores of the ARC high performance computing facilities at the University of Leeds. This time was chosen somewhat arbitrarily, but is at a time when the initially rapid flow changes have passed and the pipe outflow conditions are smoothly reducing with time, such that an assumption of a sequence of steady states is not unreasonable - it takes fractions of a second to reach a steady state in the simulation, and the inlet conditions change by no more than 1% from  $t = 35$  s to  $t = 49$  s. The inflow conditions are listed in Table 1. The inflow is introduced into the numerical domain in the region defined at the pipe end as a semi-circle with radius  $r = 0.075$  m in the vertical  $x$ - $z$  planes centred at  $x = 0$  m,  $y = 1.5$  m and  $z = -0.375$  m for  $x > 0$ . Pressure and temperature define phase densities from the equation of state, which result in a combined mixture density according to the condensed phase fraction. Outflow velocity is set in such a way as to ensure the mass-flow rate emerging from the whole pipeline is that predicted by DNV GL. These pipeline inflow conditions are enforced on every step in this region. At this time we have not included water vapour in the model. We discuss the implications of this in later sections. The initial state of the fluid in the rest of the domain consists entirely of stationary dry air at a pressure and temperature given in Table 1. Conditions in air are calculated via an ideal

gas equation of state with  $\gamma_a = 7/5$ . The near-field Mach shock structure, flow in the crater and flow immediately above the crater was considered in a single simulation, hence the high cost of accurately resolving the expansion zone and shock structure, as well as the rest of the flow through the crater. This approach neglects the effects of a cross-flow in the atmosphere, but is a reasonable approximation to make over the region up to a few metres above the crater, where the momentum from the release dominates; we have also tested the effect of cross-winds elsewhere Wareing et al. (2014b) and demonstrated that at 1 m above the crater, any cross-wind has little to no effect on the momentum-dominated outflow from the crater.

The upper  $x = 3.0$  m,  $y = 3.0$  m and  $z = 3.0$  m boundaries were all set to free-flow, introducing air with the initial atmospheric condition if an in-flow was detected. The lower  $x$  and  $y$  boundaries at  $x = 0$  m and  $y = 0$  m were symmetry boundaries. Below  $z = 0$  m, the crater was defined as a solid wall according to the measurements in Figure 1. Given that vortex structures may be present in the flow as it reaches steady state and air is dragged into the simulation grid above the pipe ends as the CO<sub>2</sub> plume flows upwards out of the crater, inflow can occur at the free-flow boundaries. Hence the boundary conditions are adjusted to ensure that only ambient air can flow into the domain, with the same properties as the initial condition, and no CO<sub>2</sub>.

## 5. Results

Figure 3 shows the predicted steady state flow in the crater on a vertical slice through the centre of the crater, parallel to the pipeline and initial

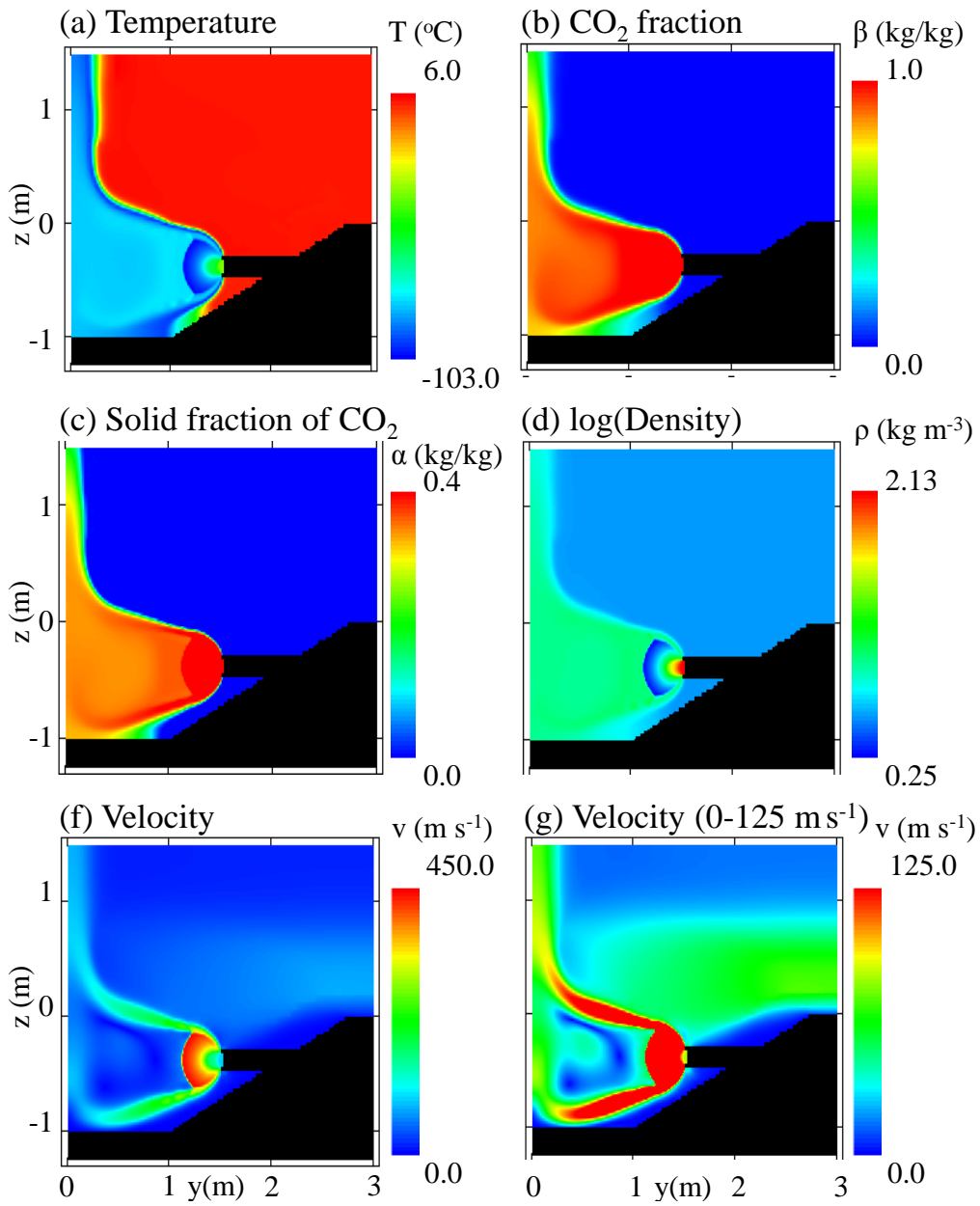


Figure 3: Numerical simulation. Vertical slices on the  $x = 0\text{m}$  plane through the centre of the crater, parallel to the pipeline, showing the steady state flow in the simulation.

velocity vector, on the  $x = 0$  m plane. The expansion zone as the fluid exits the pipeline is clear. In this region, the lowest temperatures of below  $-100^{\circ}\text{C}$  are reached just before the Mach shock, considerably below the triple point at  $-56.6^{\circ}\text{C}$ . Liquid  $\text{CO}_2$  drops solidify into dense solid  $\text{CO}_2$  particles. Just before the Mach shock at the termination of this expansion zone, the highest velocities approaching  $450 \text{ m s}^{-1}$  (and lowest pressures) are reached. Beyond the Mach shock, the temperature in the flow is at the sublimation temperature of  $-78.9^{\circ}\text{C}$  as the homogeneous equilibrium model necessitates this if solid and gas phases are present in pure  $\text{CO}_2$ . The temperature drops slightly as air is mixed into the jet, particularly as the jets from each end interact in the middle of the crater (on the  $y = 0$  m plane). The solid fraction just beyond the Mach shock is around 0.35 and by the time the flow reaches the location of the measuring plane above the crater, this has dropped only slightly to 0.3 - solid  $\text{CO}_2$  is flowing out of the crater into the dispersing plume. The core and sheath nature of the initial sonic jet before the interaction is clear in the plot of velocity, where the slice through the jet shows the slow moving core surrounded by the fast moving sheath, before the interaction with the opposite jet is clear approaching the  $y = 0$  m symmetry axis (the left side of the plotted domains). On interaction, the flow is spread out perpendicular to the original pipeline (and to these plots), with the majority of the flow going upwards. The rest of this lateral flow is then spread upwards as the flow runs up the crater walls and leaves the crater inclined at the crater wall angle. The second velocity plot shows in more detail that air is entrained into the crater from behind the pipeline rupture at a considerable rate up to  $50 \text{ m s}^{-1}$ . Apart from in the pipeline

and in the expansion region, the pressure in the entire domain is within a few percent of atmospheric levels.

Figure 4 shows the flow on a horizontal plane 1m above the crater. The highest CO<sub>2</sub> fractions, densities and magnitudes of velocity are in a narrow fan directed upwards in the centre of the crater (at the origin (0,0)) and in the lateral spread of the flow turned upwards by interaction with the crater wall at  $x > 1.5$  m axis. As the jet still contains approximately 30% solid CO<sub>2</sub>, the mixture (air & CO<sub>2</sub>) temperature in this equilibrium model is below the sublimation temperature. The peak velocity magnitude is around 80 m s<sup>-1</sup>, in the centre of the crater. It's also clear in the slice showing the magnitude of velocity that air is entraining into the crater at approximately 25 m s<sup>-1</sup>. The majority of the air flow into the crater is below this level, as highlighted in the previous figure. The boundary conditions have ensured that only ambient air with the initial condition has been dragged into the simulation on the upper boundary at  $y = 3$  m. The pressure in all the slices shown in Figure 4 is within a few percent of atmospheric levels.

Figure 5 shows a plot of experimental data (markers, coloured online according to the temperature scale) on the horizontal plane 1 m above the crater with the results of the numerical simulation (contour plot, coloured online according to the same temperature scale). The experimental data was averaged over the period 30 s to 60 s (300 individual measurements) in order to obtain averaged experimental observations in order to compare to the RANS solution. The slice from the simulation, performed in a quarter crater, was reflected about both the  $x$  and  $y$  axes in order to obtain a prediction covering the domain for comparison with the experimental data.

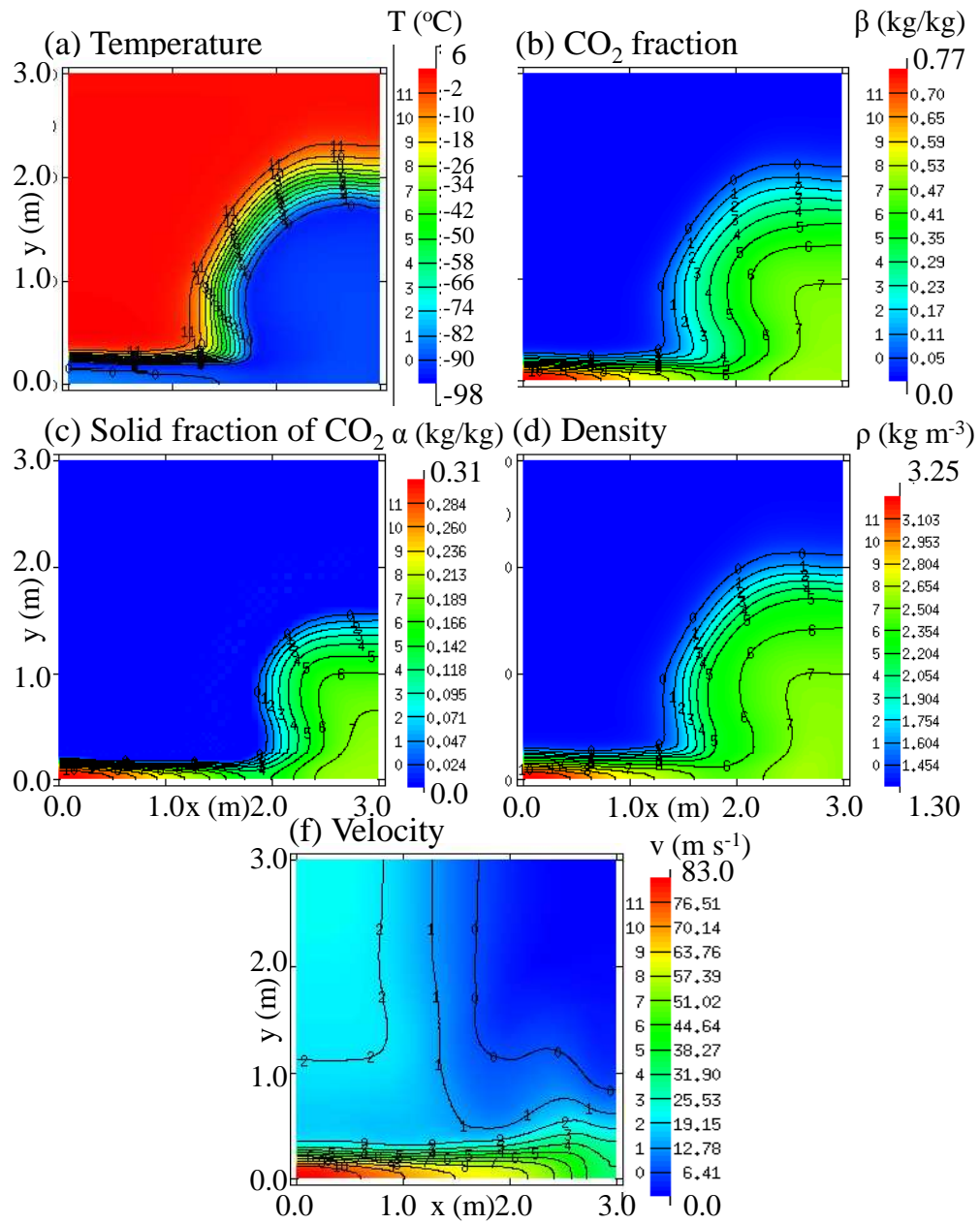


Figure 4: Numerical simulation. Horizontal slices at  $z = 1\text{m}$  above the crater, showing the steady state flow out of the crater.

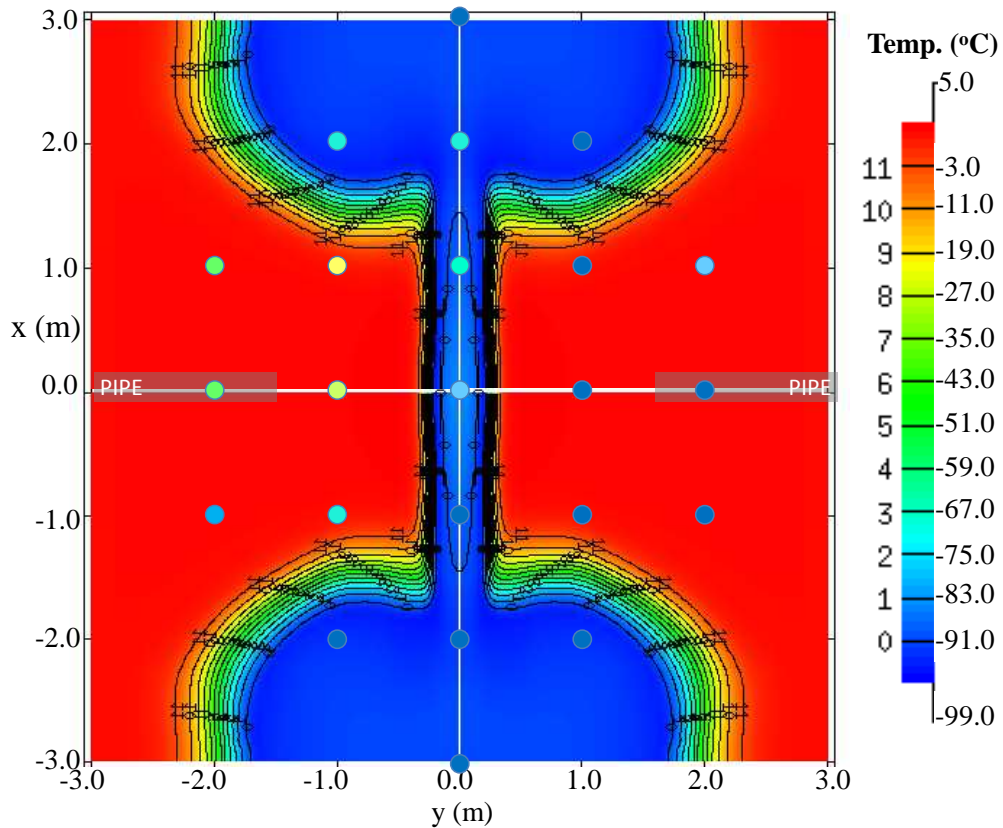


Figure 5: A comparison of experimental data (markers) with simulated prediction (contour plot) on a two-dimensional plane 1m above the crater ( $z = 1$  m). Experimental data and prediction are colour-coded online according to the temperature scale. The quarter crater prediction (upper right) was reflected twice in order to create this figure.

The first thing to note from the figure is that there is good agreement between experiment and prediction with regard to the range of temperatures predicted in the flow. The numerical simulation is able to reproduce the low temperatures around  $-100^{\circ}\text{C}$  seen in the experimental data. With regard to the structure of the flow, in the prediction, the balanced flows from each pipe

inlet meet below this plane in the centre of crater and interact, sending the flow sideways and upwards off the base of the crater in a semicircular fan, perpendicular to the pipeline. Directly above the interaction region, through the plane of interest here, this flow goes upwards relatively undisturbed in the centre of the crater and hence is narrowly confined along the pipeline direction, spreading in the fan perpendicular to the pipeline direction. At the sides, perpendicular to the pipeline, as the fan hits the crater walls below this plane, it is deflected and spread up and along the crater walls, dispersing more widely and resulting in larger, cold cloud lobes on the plane of interest shown in Figure 5. The experimental data is broadly in agreement with this structure - the cold and warm regions are roughly equivalent. However, it should be noted that along the pipeline axis, the experimental flow is considerably wider than expected and the coldest temperature is reached closer to the pipe inlet at positive  $y$ . Cold lobes appear to be present in the experimental data. The suggestion that one flow may be going over the top of the other and out of the crater along the ground in either pipeline direction, which could be supported by this experimental data, is ruled out by photographic and video evidence of the release confirming a plume coming upwards out of the crater.

In Figure 6, experimental data and numerical predictions are presented along sections (lines) of constant  $x$  on the same plane at  $z = 1$  m above the crater. This figure is designed to elucidate whether the flow emerging from the crater is in the centre of the crater ( $y = 0$  m) or offset toward either pipe end. These sections are parallel to the pipeline. The predicted narrow nature of the cold fan perpendicular to the pipeline is clear in the

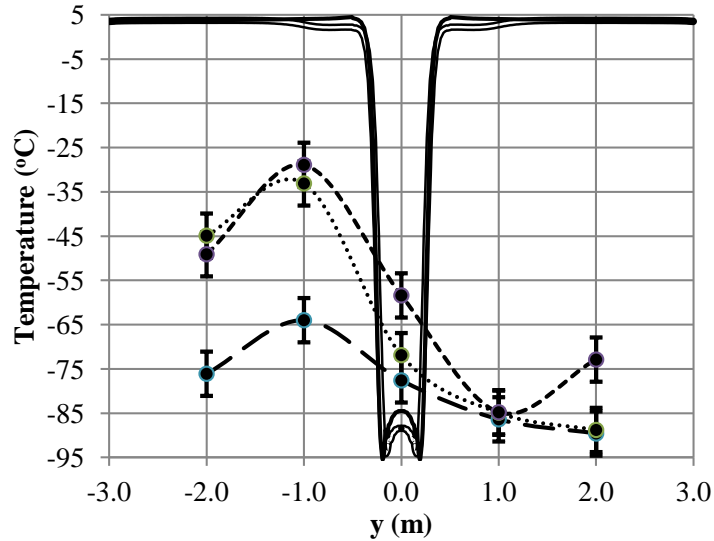


Figure 6: A comparison of experimental data with simulated prediction on cuts across the measuring plane, parallel to the pipeline. The experimental data is presented at  $x = -1$  m (long dashed line connecting markers), at  $x = 0$  m (dotted line connecting markers) and at  $x = 1$  m (short dashed line connecting markers). The simulated prediction is presented at  $x = 0$  m (solid line) and, almost overlaying it, at  $x = 1$  m (double solid lines) which is equivalent to  $x = -1$  m due to the use of symmetries in the simulation.

very confined region of very low temperature for all predictions. Shown are three sections through the experimental data on this plane, at  $x = -1$  m,  $x = 0$  m and  $x = 1$  m. Error bars represent the accuracy of the sensors in this range, discussed earlier:  $\pm 5^\circ\text{C}$ , which in almost all cases is at least a factor to two greater than the standard deviation of the data for each sensor during the 30s averaging period. In the experimental data, the coldest region considering all three cuts through the experimental data is towards the pipe inlet at positive  $y$ , specifically at  $y = 1$  m. Given that the photographic data indicates there is a plume coming out of the crater, these data appear to

indicate that the flow is not coming out of the centre of the crater, but is in fact moved towards the pipe inlet at positive  $y$ .

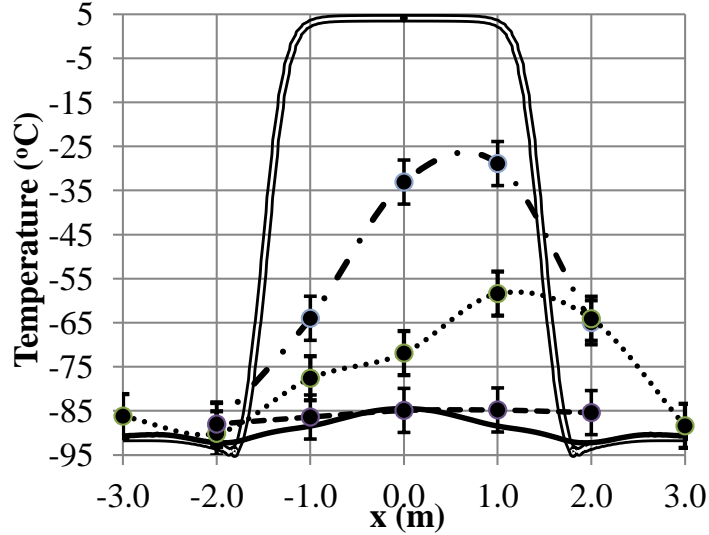


Figure 7: A comparison of experimental data with simulated prediction on cuts across the measuring plane perpendicular to the pipeline. The experimental data is presented at  $y = -1$  m (dot-dashed line connecting markers)  $y = 0$  m (dotted line connecting markers) and at  $y = 1$  m (dashed line connecting markers). The simulated prediction is presented at  $y = 0$  m (solid line) and at  $y = 1$  m (double solid lines), which is equivalent to  $y = -1$  m due to the use of symmetries in the simulation.

Considering sections on the measuring plane perpendicular to the pipeline above the crater, Figure 7 presents experimental data and numerical prediction along sections of constant  $y$ . The numerical prediction shown is through the core of the cold fan and lobes of the dispersing cloud ( $y = 0$  m) and outside the fan, but still intersecting the cold lobes of the flow ( $y = 1/ -1$  m). The prediction indicates that in ‘fan-like’ flow out of the crater, the flow should be cold across the entire measurable range on the plane. At

$y = 1/ - 1$  m, the cut through the prediction contains ambient air (no CO<sub>2</sub>) in the range  $-1 < x < 1$  m. Outside this range, it intersects the cold CO<sub>2</sub> lobes generated above the crater walls. The dotted line in the figure connects the experimental data (markers) across the centre of the crater at  $y = 0$  m. The temperatures are up to 25°C warmer than the prediction around  $x = 1$  m, but drop toward the predicted colder temperatures at larger  $|x|$  - indicating this cut is not through the centre of the plume. Experimental data on the section through the crater at  $y = -1$  m shows an even greater range of temperatures - around -30°C at  $x = 1$  m, again dropping fast toward the predicted colder temperatures at larger  $|x|$ . Interpretation of these data in light of the numerical prediction would suggest that both these sections are cutting into cold lobes at larger  $|x|$ , although they are clearly in a mixed medium between cold CO<sub>2</sub> and ambient air in the region  $-1 \text{ m} < x < 1 \text{ m}$ . Turning to the the experimental data on the section at  $y = 1$  m (dashed line connecting markers), these data are consistently cold across the crater. This is in agreement with the predicted behaviour across the core of the fan (the solid line prediction) - including excellent agreement at the position of the pipeline ( $x = 0$ ) and the presence of the same data trend, cooling away from the centre of the crater as more air is mixed into the plume. It is possible to conclude based on these parallel cuts, that the experimental data indicates that the flow is emerging from the crater at  $y = 1$  - i.e. moved over towards the pipe inlet at positive  $y$ . The experimental data also indicates that the plume is considerably wider than predicted, parallel to the pipeline, which may be a result of turbulence or flapping of the jet, or in reality unbalanced pipe flows - discussed further in the next section.

## 6. Discussion

Why is the observed upwards flow not as narrow as the prediction? Why is the coldest region moved towards the Eastern pipe (the right side of Figure 5)? The specification of this experiment was for balanced flow. Later closer inspection of the experimental apparatus and procedure on the day this experiment took place revealed two things (DNV GL, private communication). Firstly, there was in fact a half-degree incline in the pipeline, which means a 2m difference in height between the opposite ends of the pipe. Secondly, there was a temperature difference between the two reservoirs when the remote valves were triggered to begin the experiment. Pressure traces indicate that close to the pipe outlets where it was assumed that the pressure would be the same at the pipe ends - i.e. balanced flow, there was actually a 3bar (25%) difference between the pressure measurements; close to the pipe end at positive  $y$ , higher pressures were measured in the pipeline than at the same location close to the pipe end in the pipeline at negative  $y$ . The flow out of the crater would appear to have been moved over towards the higher pressure pipe inflow by this pressure difference at the pipe ends. Part II of this series will examine this situation and demonstrate that unbalanced pipe flows can both widen the plume and shift it towards either the higher or lower pressure pipe inlet. In general then, the model has been able to predict the behaviour in this scaled experiment reasonably well, predicting the nature, if not the exact location of the cold plume and wider lobes of the flow on the plane 1 m above the crater. The differences in the location of the plume can be understood as a result of unbalanced flows in the experiment. Unbalanced flow could also explain the observed wide nature of the plume compared to

the predicted narrow fan.

In this case the rupture was into air in a pre-formed crater. The dimensions of the crater were based on experimental observations of other craters formed in the same experimental programme. A different depth of cover would result in a different crater shape, which may also affect the collimation of the flow out of the crater.

## **7. Limits of applicability**

It has been demonstrated in the previous sections that the model can now predict the characteristics of ruptures of below ground pipelines, with inconsistencies that can be understood in terms of experimental procedure. These predictions have required a complex equation of state which accounts not only for accurate behaviour in the gas phase, but also, because of the temperature range from the release point into the far-field, for accurate behaviour in the liquid and solid phases and the transition to the solid phase. Tests with a simpler two-phase equation of state - the Peng and Robinson equation (Peng and Robinson, 1976) - have shown that it is unable to predict core temperatures or solid fractions in the near-field. Tests with an ideal equation of state have shown it is entirely unsuitable for this near-field application. For further details, the reader is referred to Wareing et al. (2013a). The results presented herein (and in our previous publications) demonstrate that those considering modelling the dispersion of CO<sub>2</sub> into the far-field must either use a suitable model in the near-field or employ predictions from a suitable model to start their far-field simulations, set-up in such a way to represent the thermodynamic complexity of the near-field. There is debate over the

precise value of the latent heat of fusion that should be used. The DIPPR<sup>®</sup> Project 801 database (<http://www.aiche.org/dippr/>), the most up to date source, states 204,932 J/Kg. Jager and Span (2012) state a value of 8.875 kJ/mol or 201,704 J/Kg. These two values are not considerably different, and so do not make much difference to the type of predictions shown. What is considerably different between the DIPPR database and Jager and Span (2012), however, is the specific heat and, therefore, the variation of internal energy with temperature, which is important to numerical approaches such as those considered here. Future work planned in this area will examine how this affects fractions of solid CO<sub>2</sub> in these flows and, more specifically, the immediate post Mach shock condensed mass fraction and will compare the performance of these two methods to that derived from molecular modelling theory.

Water vapour in the atmosphere will also affect the flow, but have limited bearing on the near-field in this definition. Predictions indicate that a free jet is entirely CO<sub>2</sub> until approximately 40 release diameters downstream from the release point. Any water vapour in the air cannot affect the core whilst it is 100% CO<sub>2</sub>, so it is not able to have an effect on the Mach shock region as that is always pure CO<sub>2</sub> within 10 release diameters of the release point. Given the likely size of craters formed in pipeline ruptures, it is unlikely to strongly affect the flow *in the crater* of a full-scale rupture. Once air does begin to mix into the core, water ice will form in the low temperature environment and since water has a latent heat of fusion greater than that of CO<sub>2</sub>, it will be an energy sink and the CO<sub>2</sub> jet itself will not be as cold as a consequence. Also, the jet plume going into the far-field formed will be more

buoyant.

Re-entrainment of CO<sub>2</sub> back into a crater has been considered previously in two ways. Taking far-field predictions, a mixture containing 15% CO<sub>2</sub> and 85% air was allowed to flow into the simulation domain in previous puncture studies (Wareing et al., 2014b), at ambient temperatures and pressures as predicted by the far-field simulation. This appeared to have no effect on the crater outflow. In the second examination, a simplified two dimensional simulation of a stalling plume was considered, as the full simulation is not possible with a near-field model alone. The results have shown that plume height is affected - it drops by one third as the cold cloud is re-entrained into the flow. Further full far-field simulations modelling the crater and employing near-field predictions, just past the Mach shock but before the interaction region in the crater, as input could be used to explore this issue further. It is possible to say from the tests conducted, however, that re-entrainment of ambient temperature, low concentration dispersing CO<sub>2</sub> into the crater has little effect on a crater outflow, but re-entrainment of a stalling plume, containing high concentration, cold CO<sub>2</sub> does have an effect on the plume, leading to a lower levels of momentum in the plume and a lower stalling height.

A homogeneous equilibrium model has also been used throughout the simulations presented here. In the case of ruptures, this is entirely applicable, as discussed in detail elsewhere (Wareing et al., 2013b), since the particles are small enough to be in equilibrium with the flow and follow the flow streamlines, considering thermal and dynamical relaxation times and distances for typical particle release velocities.

The choice of turbulence model has a bearing on the predictions. These simulations have employed the  $k - \epsilon$  turbulence model with a compressibility correction required by the decompression of the underexpanded pipeline flow. We have shown previously that this model is capable of modelling free releases into air (Wareing et al., 2014a). To ensure compatibility within the COOLTRANS research programme, we continued to employ this model for the below ground releases, with good results for punctures compared to experimental data (Wareing et al., 2014b). However, a Reynolds-stress turbulence model would be more appropriate for these situations. Even with such a second-moment turbulence closure, it is not possible to capture the true transient turbulent nature of these releases with a RANS model, as the model is *time-averaged* predicting a time-averaged structure. Large eddy simulation could be advantageously employed, and may predict wider flows exiting craters, but questions then have to be answered as to how this would link with pipe-flow and far-field models and feed into the RANS methods common in industry.

The depth and type of soil cover has an important bearing on the behaviour of a rupture, in particular on the shape and dimensions of the crater generated in a rupture. Further simulations, reported in Part II of this series, examine the variation of pipeline soil cover, including depth and type, through variation of the pre-formed craters employed. That said, the case of ruptures forming their own craters in simulations is worth further consideration, but is beyond the scope of this project.

## 8. Conclusions

This article has presented a novel method for simulating sonic high pressure releases of dense phase CO<sub>2</sub> from the rupture of a buried pipeline. This approach has been validated against limited available experimental data. The model is capable of predicting temperatures, structures and behaviour in the crater outflow in broad agreement with those data, obtained as part of the COOLTRANS research programme (Cooper, 2012). Inconsistencies between the prediction and experimental data can be explained in terms of unbalanced flow into the crater, when balanced flow was assumed for the ‘data-blind’ simulation. This near-field prediction has required a three-phase accurate equation of state, that also accounts for the latent heat of fusion. Further experimental data at both laboratory-scale and larger scales is required to further validate the model and shed light on the behaviour of solid CO<sub>2</sub> in and around the crater.

In the second part of this two-paper series on ruptures of buried CCS pipelines, this model will be applied to the numerical simulation of a rupture of a full-scale pipeline. Since no near-field experimental data close to, or just above, the crater is available for full-scale ruptures, a sensitivity study examining a range of different crater profiles will also be examined. Integrated fluxes and estimates of solid deposition will be presented in order to provide robust far-field source conditions for further CFD and quantified risk assessment.

## Acknowledgements

During the undertaking of this work (2011-2013), CJW was supported by the COOLTRANS research programme (Cooper, 2012) co-funded by National Grid, and CJW and MF would like to thank National Grid and the European Union for their support of the work described herein. We acknowledge the provision of information regarding the experiments from DNV GL (D. Allason, K. Armstrong and R.P. Cleaver). We acknowledge a useful critique from the anonymous referee which improved the original manuscript and suggested the division into two more detailed parts. National Grid initiated the COOLTRANS research programme as part of the Don Valley CCS Project in order to address knowledge gaps relating to the safe design and operation of onshore pipelines for transporting dense phase CO<sub>2</sub> from industrial emitters in the UK to storage sites offshore. The Don Valley CCS Project is co-financed by the European Union's European Energy Programme for Recovery (EEPR). The sole responsibility of this publication lies with the authors. The European Union is not responsible for any use that may be made of the information contained therein. The numerical simulations were carried out on the STFC-funded DiRAC I UKMHD Science Consortia machine and the N8 HPC machine provided and funded by the N8 consortium and EPSRC (Grant No.EP/K000225/1). Both are hosted as part of and enabled through the ARC HPC resources and support team at the University of Leeds (A. Real, M. Dixon, M. Wallis, M. Callaghan & D. El-Moghraby).

## References

- Ahmad, M., Bögemann-van Osch, M., Buit, L., Florisson, O., Hulsbosch-Dam, C., Spruijt, M., Davolio, F., 2013. Study of the thermohydraulics of CO<sub>2</sub> discharge from a high pressure reservoir. *Int. J. Greenhouse Gas Control* 19, 63–73.
- Allason, D., Armstrong, K., Cleaver, P., Halford, A., Barnett, J., 2012. Experimental studies of the behaviour of pressurised release of carbon dioxide. In: *ICChemE Symposium Series No. 158, ICChemE*. pp. 142–152.
- Cooper, R., 2012. National Grid's COOLTRANS research programme. *Journal of Pipeline Engineering* 11, 155–172.
- Cosham, A., Jones, D.G., Armstrong, K., Allason, D., Barnett, J., 2012. The decompression behaviour of carbon dioxide in the dense phase. In: *ASME Proc. 45141. The Proceedings of the 2012 9th International Pipeline Conference IPC2012 v. 3, ASME*. pp. 447–464.
- Cosham, A., Jones, D.G., Armstrong, K., Allason, D., Barnett, J., 2012b. Ruptures in gas pipelines, liquid pipelines and dense phase carbon dioxide pipelines. In: *ASME Proc. 45141. The Proceedings of the 2012 9th International Pipeline Conference IPC2012 v. 3, ASME*. pp. 465–482.
- Cumber, P.S., Fairweather, M., Falle, S.A.E.G., Giddings, J.R., 1994. Predictions of the structure of turbulent, moderately underexpanded jets. *Journal of Fluids Engineering* 116, 707–713.

- Cumber, P.S., Fairweather, M., Falle, S.A.E.G., Giddings, J.R., 1995. Predictions of the structure of turbulent, highly underexpanded jets. *Journal of Fluids Engineering* 117, 599–604.
- Cumber, P.S., 2001. Predicting outflow from high pressure vessels. *Trans IChemE* 79, Part B, 13–22.
- Dixon, C.M., Gant, S.E., Obiorah, C., Bilio, M., 2012. Validation of dispersion models for high pressure carbon dioxide releases, in: *IChemE Symposium Series No. 158, IChemE*. pp. 153–163.
- Dixon, C.M., Hasson, M., 2007. Calculating the release and dispersion of gaseous, liquid and supercritical CO<sub>2</sub>, in: *IMEchE Seminar on Pressure Release, Fires and Explosions, London, IMechE*.
- Dixon, C.M., Heynes, O., Hasson, M., 2009. Assessing the hazards associated with release and dispersion of liquid carbon dioxide on offshore platforms, in: *8th World Congress of Chemical Engineering, Montreal*.
- Falle, S.A.E.G., 1991. Self-similar jets. *Monthly Notices of the Royal Astronomical Society* 250, 581–596.
- Falle, S.A.E.G., 2005. AMR applied to non-linear elastodynamics, in: Plewa, T., Linde, T., Weirs, V.G. (Eds.), *Proceedings of the Chicago Workshop on Adaptive Mesh Refinement Methods, Springer Lecture Notes in Computational Science and Engineering v.41, Springer, New York U.S.A.* pp. 235–253.
- Gant, S.E., Narasimhamurthy, V.D., Skjold, T., Jamois, D., Proust, C., 2014. Evaluation of multi-phase atmospheric dispersion models for application

- to Carbon Capture and Storage. *Journal of Loss Prevention in the Process Industries* 32, 286–298.
- Godunov, S.K., 1959. A difference scheme for numerical computation of discontinuous solutions of equations of fluid dynamics. *Matematicheskii Sbornik* 47, 271–306.
- Harten, A., Lax, P.D., van Leer, B., 1983. On upstream differencing and Godunov-type schemes for hyperbolic conservation laws. *SIAM Review* 25, 35–61.
- Hill, T.A., Fackrell, J.E., Dubal, M.R., Stiff, S.M., 2011. Understanding the consequences of CO<sub>2</sub> leakage downstream of the capture plant. *Energy Procedia* 4, 2230–2237.
- Hulsbosch-Dam, C.E.C., Spruijt, M.P.N., Necci, A., Cozzani, V., 2012a. As approach to carbon dioxide particle distribution in accidental releases. *Chemical Engineering Transactions* 26, 543–548.
- Hulsbosch-Dam, C.E.C., Spruijt, M.P.N., Necci, A., Cozzani, V., 2012b. Assessment of particle size distribution in CO<sub>2</sub> accidental releases. *J. Loss Prevention in the Process Industries* 25, 254–262.
- Jager, A., Span, R., 2012. Equation of State for Solid Carbon Dioxide Based on the Gibbs Free Energy. *Journal of Chemical & Engineering Data* 57, 590–597.
- Liu, Y., Calvert, G., Hare, C., Ghadiri, M., Matsusaka, S., 2012b. Size measurement of dry ice particles produced from liquid carbon dioxide. *Journal of Aerosol Science* 48, 1–9.

- Liu, X., Godbole, A., Lu, C., Michal, G., Venton, P., 2014. Source strength and dispersion of CO<sub>2</sub> releases from high-pressure pipelines: CFD model using real gas equation of state. *Applied Energy* 126, 56–68.
- Mazzoldi, A., Hill, T., Colls, J.J., 2008a. CFD and Gaussian atmospheric dispersion models: a comparison for leak from carbon dioxide transportation and storage facilities. *Atmos. Environ.* 42, 8046–8054.
- Mazzoldi, A., Hill, T., Colls, J.J., 2008b. CO<sub>2</sub> transportation for carbon capture and storage: sublimation of carbon dioxide from a dry ice bank. *International Journal of Greenhouse Gas Control* 2, 210–218.
- Mazzoldi, A., Hill, T., Colls, J.J., 2011. Assessing the risk for CO<sub>2</sub> transportation within CCS projects, CFD modelling. *International Journal of Greenhouse Gas Control* 5, 816–825.
- Peng, D.Y., Robinson, D.B., 1976. A new two-constant equation of state. *Industrial and Engineering Chemistry: Fundamentals* 15, 59–64.
- Sarkar, S., Erlebacher, G., Hussaini, M.Y., Kreiss, H.O., 1991. The analysis and modelling of dilatational terms in compressible turbulence. *Journal of Fluid Mechanics* 227, 473–493.
- Span, R., Wagner, W., 1996. A new equation of state for carbon dioxide covering the fluid region from the triple-point temperature to 1100 K at pressures up to 800 MPa. *Journal of Physical and Chemical Reference Data* 25, 1509–1596.
- van Leer, B., 1977. Towards the ultimate conservative difference scheme.

- IV. A new approach to numerical convection. *Journal of Computational Physics* 23, 276–299.
- Wareing, C., Fairweather, M., Falle, S.A.E.G., Woolley, R.M., 2012. Reynolds-averaged Navier-Stokes modelling of sonic CO<sub>2</sub> jets, in: Hanjalic, K., Nagano, Y., Borello, D., Jakirlic, S. (Eds.), *Proceedings of the 7th International Symposium on Turbulence, Heat and Mass Transfer*, Begell House Inc., New York. pp. 349–512.
- Wareing, C., Woolley, R.M., Fairweather, M., Falle, S.A.E.G., 2013a. A composite equation of state for the modelling of sonic carbon dioxide jets in carbon capture and storage scenarios. *AIChE Journal* 59, 3928–3942.
- Wareing, C., Fairweather, M., Peakall, J., Keevil, G., Falle, S.A.E.G., Woolley, R.M., 2013b. Numerical modelling of particle-laden sonic CO<sub>2</sub> jets with experimental validation, in: Zeidan, D. (Ed.), *AIP Conference Proceedings of the 11th International Conference of Numerical Analysis and Applied Mathematics*, AIP Publishing. pp. 98–102.
- Wareing, C., Fairweather, M., Falle, S.A.E.G., Woolley, R.M., 2014. Validation of a model of gas and dense phase CO<sub>2</sub> jet releases for carbon capture and storage application. *Int. J. Greenhouse Gas Control* 20, 254–271.
- Wareing, C., Fairweather, M., Falle, S.A.E.G., Woolley, R.M., 2014b. Modelling punctures of buried high-pressure dense phase CO<sub>2</sub> pipelines in CCS applications. *Int. J. Greenhouse Gas Control* 29, 231–247.
- Webber, D.M., 2011. Generalising two-phase homogeneous equilibrium

- pipeline and jet models to the case of carbon dioxide. *J. Loss Prevention in the Process Industries* 24, 356–360.
- Wen, J., Heidari, A., Xu, B., Jie, H., 2013. Dispersion of carbon dioxide from vertical vent and horizontal releases - a numerical study. *Proceedings of the Institution of Mechanical Engineers, Part E: Journal of Process Mechanical Engineering* 227, 125–139.
- Witlox, H.W.M., Harper, M., Oke, A., 2009. Modelling of discharge and atmospheric dispersion for carbon dioxide release. *J. Loss Prevention in the Process Industries* 22, 795–802.
- Witlox, H.W.M., Stene, J., Harper, M., Nilsen, S.H., 2011. Modelling of discharge and atmospheric dispersion for carbon dioxide releases including sensitivity analysis for wide range scenarios. *Energy Procedia* 4, 2253–2260.
- Woolley, R.M., Fairweather, M., Wareing, C.J., Falle, S.A.E.G., Proust, C., Hebrard, J., Jamois, D., 2013. Experimental measurement and Reynolds-averaged Navier-Stokes modelling of the near-field structure of multi-phase CO<sub>2</sub> jet releases. *Int. J. Greenhouse Gas Control* 18, 139–149.
- Woolley, R.M., Fairweather, M., Wareing, C.J., Proust, C., Hebrard, J., Jamois, D., Narasimhamurthy, V.D., Storvik, I.E., Skjold, T., Falle, S.A.E.G., Brown, S., Mahgerefteh, H., Martynov, S., Gant, S., Tsangaris, D.M., Economou, I.G., Boulougouris, G.C., Diamantonis, N.I., 2014. An integrated, multi-scale modelling approach for the simulation of multi-

phase dispersion from accidental CO<sub>2</sub> pipeline releases in realistic terrain.  
Int. J. Greenhouse Gas Control 27, 221–238.

Table 1: Initial conditions, courtesy of DNV GL.

Reservoir conditions	
Pressure	13.5 MPa
Temperature	5.0 °C
CO <sub>2</sub> fraction	1.0
Condensed phase fraction	1.0
Atmospheric conditions	
Pressure ( $P_a$ )	0.0985 MPa
Temperature ( $T_a$ )	7.7 °C
Velocity ( $u_a$ )	4.5 m s <sup>-1</sup>
Wind bearing	250 °C
Pipe exit conditions	
Pressure ( $P_i$ )	1.196 MPa
Temperature ( $T_i$ )	-35.1 °C
Mass-flow rate ( $M_i$ )	146.5 kg s <sup>-1</sup>
CO <sub>2</sub> fraction ( $\beta_i$ )	1.0
Liquid fraction ( $\alpha_i$ )	0.79